

# Orientational and conformational correlations in deformed polymer chains with fixed end-to-end separation: A Brownian dynamics simulation study

Turkan Haliloglu, Ivet Bahar, and Burak Erman

*Polymer Research Center and School of Engineering, Bogazici University, Bebek 80815, Istanbul, Turkey*

(Received 20 April 1992; accepted 26 May 1992)

Static and dynamic correlations between bond conformations and reorientations are examined by the Brownian dynamics simulation technique for polymer chains with fixed ends. Polyethylenelike model chains are considered. Rates of rotational isomeric transitions and time evolution of orientational correlations are analyzed for various extensions of the chain. The more extended chains exhibit the highest mobility in the short-time scale but possess the lowest effective rate of rotational isomerization as follows from a hazard analysis covering time ranges up to 10 ns. The time decays of bond orientational correlations are reproducible by stretched exponential functions with exponent almost independent of chain extension. The imposition of fixed deformation at chain ends affects the orientational mobility of the chain down to the scale of individual bonds which may be observed from the biased evolution of time-dependent distribution functions for bond spatial reorientations.

## I. INTRODUCTION

Previous theoretical considerations indicate that polymers with fixed ends are subject to distinct conformational statistics, depending on the degree of extension or perturbation of the chain.<sup>1</sup> Similarly, the local reorientational and conformational dynamics of deformed chains is expected to be altered due to the imposition of spatially constrained ends. Examination of the distribution of conformational states and their time evolution in chains with fixed end-to-end separation  $r$  is expected to give some insights as to the intrinsic orientational characteristics of deformed network chains.

A potentially useful tool to study high-frequency motions and associated dynamic properties in polymeric systems is the Brownian dynamics (BD) simulation technique.<sup>2</sup> The time evolution of particles in BD method is described by coupled Langevin differential equations or alternatively stochastic difference equations which are shown to be equivalent to the Fokker-Planck description of particle diffusion.<sup>3,4</sup> Earliest studies using this technique adopted simple model chains such as one-dimensional bistable oscillators.<sup>5,6</sup> Studies of more realistic moderate size chains with fixed bond lengths and bond angles were soon performed by Fixman using generalized coordinates,<sup>3,4</sup> by Pear and Weiner,<sup>7,8</sup> and Levy *et al.*<sup>9</sup> In the BD study of conformational transitions by Helfand, Wasserman, and Weber,<sup>10,11</sup> bond stretching and bond-angle bending were incorporated as possible degrees of freedom in addition to bond torsional mobility. BD has thereafter proven to be a mathematically convenient method to treat several problems involving (i) static properties such as end-to-end distribution functions in various regimes,<sup>12</sup> surface adsorption,<sup>13</sup> and collapse transition produced by modulating intermolecular interactions,<sup>14</sup> and (ii) dynamic phenomena such as relaxation of various correlation functions, transitions between rotational conformers,<sup>10,11,15</sup> chain diffusion,<sup>4,16</sup> and cyclization.<sup>17</sup> Moreover, the time

evolution of internal relaxational modes and dynamic light scattering functions has been recently investigated by the BD method,<sup>18</sup> following the formalism introduced by Ermak and McCammon<sup>19</sup> which considers the effect of fluctuating hydrodynamic interactions.

In the present study, BD simulations are performed using the polyethylenelike model chain of Helfand, Wasserman, and Weber.<sup>10,11</sup> A similar mathematical formalism has been recently adopted by Adolf and Ediger<sup>20</sup> to analyze the role of cooperativity in conformational transitions of polyisoprene. The ends of the chains investigated in the present study are held fixed in space, to mimic the state of deformed chains following the affine network model. The simulations are repeated for various end-to-end separations to assess the influence of chain extension (or compression) on the conformational and orientational behavior of the chain. The paper is organized as follows. The model and the method are described in Sec. II. In Sec. III the BD trajectories of bond dihedral angles are displayed for chains of various extension and the rotational isomerization rates are estimated from hazard analysis. Static and dynamic correlations between bond orientations are analyzed. The time evolution of probability distribution functions for bond dihedral angles and bond reorientation in space are obtained. In Sec. IV concluding remarks are presented.

## II. MOLECULAR MODEL AND SIMULATION METHOD

### A. Model description

A segment  $AB$  of  $N$  bonds in a laboratory-fixed coordinate system  $OXYZ$  is considered. The two ends  $A$  and  $B$  of the chain are held fixed in space throughout the BD simulation. For mathematical convenience the first atom is assumed to coincide with the origin of the frame  $OXYZ$  and the first bond lies along the  $X$  axis. The tetrahedrally attached second bond is in the plane  $XY$  and makes an

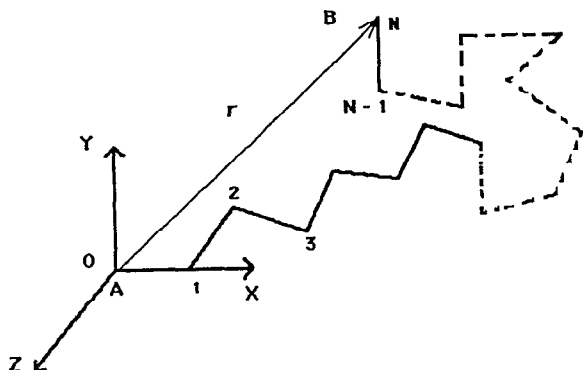


FIG. 1. Schematic representation of a chain of  $N$  bonds in a fixed reference frame OXYZ. Atoms with indices 0, 1, 2, and  $N$  are fixed in space throughout the BD simulations of a chain of a given end-to-end separation vector  $r$ .

acute angle with the  $X$  axis, as shown in Fig. 1. Holding the direction of the first two bonds fixed in space corresponds to eliminating the three degrees of freedom associated with the absolute spatial reorientation of the chain. This device is inconsequential for the study of the internal conformational and orientational dynamics of the chain which is of interest in the present study. The backbone atoms are indexed from 0 to  $N$  and their location with respect to the frame OXYZ are given by the position vectors  $\mathbf{r}_i = (x_i, y_i, z_i)$ .  $\mathbf{r}_i$  may alternatively be viewed as the position vector of the  $i$ th united group forming the chain, in which the hydrogen atoms or other substituents are collapsed into the backbone atom. For simplicity, the  $i$ th backbone atom or group will be referred to as  $C_i$ . The position vector  $\mathbf{r}_N$  of the terminal atom is equal to the end-to-end vector  $\mathbf{r}$  of the chain.

A short sequence of bonds between atoms  $C_{i-2}$  and  $C_{i+2}$  is shown in Fig. 2.  $\mathbf{l}_i$  is the bond vector connecting atoms  $i-1$  and  $i$  as

$$\mathbf{l}_i = \mathbf{r}_i - \mathbf{r}_{i-1} \quad i = 1, \dots, N. \quad (1)$$

The dot product of consecutive bond vectors defines the supplemental bond angle  $\theta_i$  as

$$\theta_i = \cos^{-1} \left( \frac{\mathbf{l}_{i+1} \cdot \mathbf{l}_i}{l_{i+1} l_i} \right) \quad i = 1, \dots, N-1, \quad (2)$$

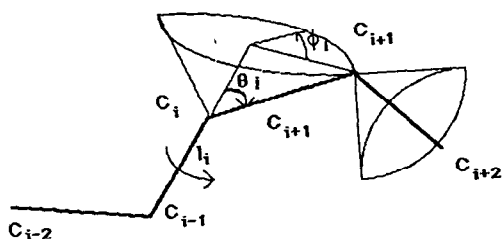


FIG. 2. A portion of simulated chain between atoms  $C_{i-2}$  and  $C_{i+2}$  indicating the generalized coordinates  $\mathbf{l}_i$ ,  $\theta_i$ , and  $\phi_i$ .  $\mathbf{l}_i$  with  $1 \leq i \leq N$  is the bond vector between atoms  $C_{i-1}$  and  $C_i$ .  $\theta_i$  is the supplemental bond angle at the  $i$ th atom and is defined in the range  $1 \leq i \leq N-1$ ,  $\phi_i$  is the torsional angle of the bonds with indices  $2 \leq i \leq N-1$ .

where  $l_i$  is the magnitude of the vector  $\mathbf{l}_i$ . The torsional state of bond  $i$  is described by the dihedral angle  $\phi_i$  which is expressed in terms of bond vectors as

$$\phi_i = \cos^{-1} \left( - \frac{(\mathbf{l}_i \times \mathbf{l}_{i-1}) \cdot (\mathbf{l}_{i+1} \times \mathbf{l}_i)}{|\mathbf{l}_i \times \mathbf{l}_{i-1}| |\mathbf{l}_{i+1} \times \mathbf{l}_i|} \right), \quad i = 2, \dots, N-1. \quad (3)$$

The values of  $0^\circ$ ,  $120^\circ$ , and  $-120^\circ$  for  $\phi_i$  define the respective rotational isometric states *trans*( $t$ ), *gauche*<sup>+</sup> ( $g^+$ ), and *gauche*<sup>-</sup> ( $g^-$ ) of bond  $i$ .<sup>1</sup>

The chain is subject to an intramolecular conformational potential controlling the changes in the bond lengths, bond angles and bond torsions in conformity with the model chains of Helfand *et al.*<sup>11</sup> The bond stretching potential  $V_b(l_i)$  for bond  $i$  is given by the harmonic function

$$V_b(l_i) = (k_b/2)(l_i - l_0)^2, \quad i = 1, \dots, N, \quad (4)$$

where  $k_b$  is the bond-stretching force constant, and  $l_0$  is the most probable bond length. Similarly,  $V_\theta(\theta_i)$  is the bond-angle bending potential which constrains the supplemental bond angle  $\theta_i$  to fluctuate about  $\theta_0$  according to

$$V_\theta(\theta_i) = (k_\theta/2)(\cos \theta_i - \cos \theta_0)^2, \quad i = 1, \dots, N-1. \quad (5)$$

Here  $k_\theta$  is the bond-angle bending force constant. The torsional motion of bond  $i$  is governed by the rotational potential  $V_\phi(\phi_i)$

$$V_\phi(\phi_i) = k_\phi \sum_{n=0}^5 a_n \cos^n \phi_i, \quad i = 2, \dots, N-1 \quad (6)$$

leading to three isomeric minima at the  $t$  and  $g^\pm$  states. Here  $k_\phi$  is the bond torsion constant and the coefficients  $a_i$  ( $0 \leq i \leq 5$ ) satisfy the relationship,

$$\sum_{n=0}^5 a_n = 0 \quad (7)$$

with  $a_0$  equal to unity. It is clear from Eq. (6) that bonds are subject to independent rotational potentials which leads to the expression

$$V_\phi(\phi_2, \dots, \phi_{N-1}) = \sum_{i=2}^{N-1} V_\phi(\phi_i) \quad (8)$$

for the rotational potential energy of the chain. Clearly, this approximation is not applicable to chains in which the rotational state of a given bond is strongly coupled to that of its close neighbors. In the case of pairwise interdependent bonds which is commonly adopted in chain statistics, the potential given by Eq. (6) should be modified as a function of two consecutive bond dihedral angles.

The total conformational potential  $V$  of the chain is given by the additive contribution of aforementioned three interactions as

$$V = \sum_{i=1}^N V_b(l_i) + \sum_{i=1}^{N-1} V_\theta(\theta_i) + \sum_{i=2}^{N-1} V_\phi(\phi_i). \quad (9)$$

## B. Brownian dynamics method

For a chain of  $N+1$  atoms each of equal mass  $m$ , the Brownian motion of the  $i$ th atom is given by the Langevin equation

$$m \frac{d^2 \mathbf{r}_i}{dt^2} = -\xi \frac{d\mathbf{r}_i}{dt} - \nabla_i V + m \mathbf{A}_i(t) \quad (10)$$

which, in the high-friction limit, reduces to the equation of motion

$$\beta \frac{d\mathbf{r}_i}{dt} = -m^{-1} \nabla_i V + \mathbf{A}_i(t). \quad (11)$$

In Eqs. (10) and (11),  $\xi$  is the friction coefficient,  $\beta$  is defined as the ratio  $\xi/m$ ,  $\nabla_i$  is the gradient operator indicating the partial derivative with respect to the position vector  $\mathbf{r}_i$ , and  $\mathbf{A}_i(t)$  is the Gaussianly distributed stochastic force per unit mass with zero mean and covariance matrix

$$\langle \mathbf{A}_i(t) \mathbf{A}_j(t') \rangle = (2\beta k_B T / m) \delta_{ij} \delta(t-t') \mathbf{I}_3. \quad (12)$$

Here  $k_B$  is the Boltzmann constant,  $T$  is the absolute temperature, and  $\mathbf{I}_3$  is the identity matrix of order 3. Explicit expressions for the stretching, bending and torsional forces resulting from the negative gradient of the potential  $V$  are given in the Appendix.

In the present model the hydrodynamic interactions between carbon centers transmitted by the surrounding medium and the intermolecular interactions between non-bonded chain units leading to excluded volume effect have not been included. The contribution of these interactions to the rapid conformational relaxation processes in polymeric chains presently investigated is expected to be negligibly small.

The Brownian dynamics simulation is performed by the numerical integration of the  $3(N+1)$  equations of motion given by Eq. (11) for each atom constituting the chain. The previously described<sup>21</sup> stochastic extension of the Runge Kutta method is adopted for that purpose and the second-order approximation is used. The integration time step is taken as  $\delta t = 0.5$  fs in conformity with previous work.<sup>11</sup> Thus, the simulated stochastic process is discrete and Markovian in the sense that the trajectories of particles are generated only at discrete time steps  $0, \delta t, 2\delta t, \dots$ , and the state of the system at a given time  $t + \delta t$  is completely determined by its state at time  $t$ .

## C. Simulation parameters

Simulations are carried out for polymeric chains of 49 bonds using the set of energy parameters listed in Table I. The parameters for torsional parameters are proposed by Ryckaert and Belleman<sup>22</sup> as a representative of a hydrocarbon chain. The force constants for bending and bond stretching were proposed by Helfand *et al.*<sup>11</sup> as a reasonable compromise between realistic estimates leading to too fast oscillations and softer potentials allowing for larger time steps of integration. The mass  $m$  of chain atoms was taken as 0.014 kg/mol, corresponding to methylene repeat units. Similarly, the equilibrium values  $l_0 = 1.53$  Å and  $\theta_0 = 70.53^\circ$  of alkane chains were used. Simulations were per-

TABLE I. Conformational energy parameters.

$k_b/m$ (ns <sup>-2</sup> )	$2.5 \times 10^9$
$k_\theta/m$ (J/kg)	$1.3 \times 10^7$
$k_\phi/m$ (J/kg)	$6.634 \times 10^5$
$a_0$	1.0
$a_1$	1.3108
$a_2$	-1.4135
$a_3$	-0.3358
$a_4$	2.8271
$a_5$	-3.3885

formed with  $\beta = 1.0 \times 10^5$ /ns for  $T = 400$  K, in general. A few runs were repeated for 300 K to estimate the effect of temperature change.

Initially, bond lengths and angles were assumed to be at their equilibrium values and bond torsional angles were assigned by the Monte Carlo technique based on the conventional rotational isomeric state<sup>1</sup> approach. Accordingly, *a priori* probabilities of rotameric states  $t$ ,  $g^+$ , and  $g^-$  were estimated from the aforementioned rotational potential and bonds are assigned isomeric states in conformity with those probabilities. Simulations were repeated for four chains with distinct end-to-end separations listed in Table II. The total duration of simulations  $t_f$  for each run are given in the third column. A given run required a CPU time of about 10–12 h on an SGI/35 Personal Iris. The end-to-end vector of each chain was held fixed by artificially freezing the two terminal atoms. This mathematical device permits to simulate a chain between two securely embedded junction points  $A$  and  $B$  in a deformed network, which undergoes restricted motions to the extent of rigidity imposed by its extension. The degree of extension of each chain is characterized by the ratio  $\lambda = r / \langle r^2 \rangle_0^{1/2}$  of its end-to-end distance  $r$  to the unperturbed chain length. Compared to the dimensions of unperturbed polyethylene chains, in which  $r \equiv \langle r^2 \rangle_0^{1/2} \approx 2.6$  nm for  $n = 49$  (using the characteristic ratio<sup>1</sup>  $C_n \approx 6.0$  in  $\langle r^2 \rangle_0 = C_n n l_0^2$ ), the simulated chains III and IV with respective end-to-end distances 3.62 and 5.23 nm have relatively expanded configurations, while the chain I with  $r = 0.97$  nm is highly contracted. The dimensions of the chain II with end-to-end distance  $r = 2.39$  nm approximate those of unperturbed polyethylene (PE) polymers.

## III. ANALYSIS OF THE TRAJECTORIES

### A. Trajectories and equilibrium distribution of bond dihedral angles

For illustrative purposes, the changes in the dihedral angles of the central bonds in the chains I, II, and IV

TABLE II. Simulation data and results.

Run	$\lambda$	$t_f$ (ns)	$p_t$	$\lambda_{ig}$ (ns <sup>-1</sup> )
I	0.37	12.0	0.593	5.60
II	0.91	13.5	0.603	5.40
III	1.38	12.5	0.642	4.58
IV	2.00	13.5	0.777	2.76

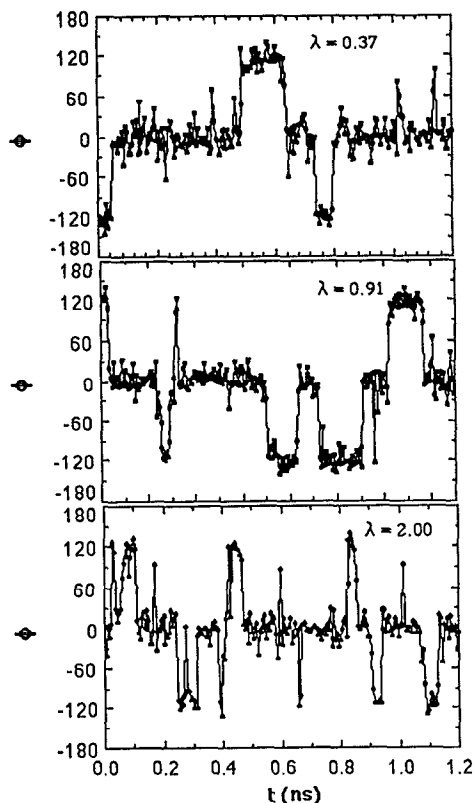


FIG. 3. Example trajectories of 1.2 ns for dihedral angles  $\phi_i$  of the central bonds in chains of various extensions, I, II, and IV with  $\lambda=0.37$ , 0.91, and 2.00, respectively, at 400 K.

during a BD simulation period of 1.2 ns are displayed in Fig. 3. The preference for rotational angles centered within  $\pm 30^\circ$  fluctuations about the isomeric states  $t$ ,  $g^+$ , and  $g^-$  is clearly apparent from those trajectories. It is noted that the more contracted chain exhibits steady transitions between rotamers while the highly strained chain with the largest  $\lambda$  is subject to fast oscillatory motions and, in particular, rapid back transitions restoring the bond torsional angle to the *trans* state, whenever the *gauche* $^\pm$  state is visited.

The normalized probability distributions of dihedral angles for the chains of various extensions are displayed in Figs. 4(a)–4(d). The distributions were obtained by considering dihedral angle intervals of  $20^\circ$ . The weak asymmetries of Figs. 4 indicate the statistical error bounds of the BD simulations. An increased preference for the *trans* state with increasing chain extension is observed. From the integration of the probability distribution curves in the ranges  $-60^\circ < \phi < 60^\circ$  and  $60^\circ < |\phi| < 180^\circ$ , the equilibrium probabilities of  $t$  and  $g^\pm$  states, respectively, are estimated. The results are listed in the fourth column of Table II. It is interesting to note from the tabulated equilibrium probabilities  $p_t$  of the *trans* state or from the curves in Figs. 4(a)–4(d) that the equilibrium distribution of rotational states is more sensitive to chain extension in the case of more stretched chains (with higher  $\lambda$ ). The contracted chain, on the other hand, exhibits a distribution of dihedral

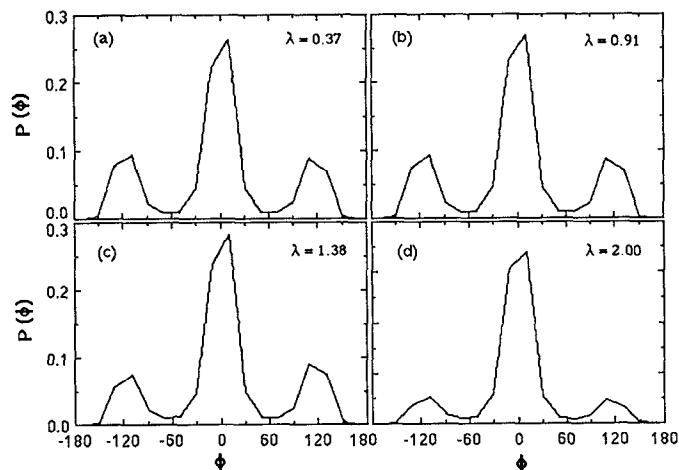


FIG. 4. Equilibrium probability distribution  $P(\phi_i)$  of dihedral angles  $\phi_i$  of internal bonds ( $5 < i < N-5$ ) for chains with (a)  $\lambda=0.37$ , (b)  $\lambda=0.91$ , (c)  $\lambda=1.38$ , and (d)  $\lambda=2.00$ .

angles that closely approximates that of the unperturbed chain.

## B. Rotational isomerization rates

For the estimation of the rotational isomerization rates in the chains with different extensions, the hazard plots shown in Figs. 5(a) and 5(b) were drawn. The cumulative hazard  $H(t)$  in the ordinate of Figs. 5 are obtained from the set of first passage times from one rotational isomeric minimum to another, by following the procedure previously outlined.<sup>6</sup> Accordingly, the first passage times are organized in ascending order and the hazard rate  $h(\tau_i)$  corresponding to the  $i$ th element  $\tau_i$  of the set of first passage times is assigned the value  $h(\tau_i) = i/(n-i)$ , where  $n$  is the total number of first passages. The cumulative hazard  $H(t)$  results from the summation of the hazard rates  $h(\tau_i)$  in the range  $0 \leq \tau_i \leq t$ .

The asymptotic slope  $\lambda$  of the cumulative hazard is a measure of the transition rate for each chain. The slope  $\lambda$  is related to the rate of transition  $\lambda_{ig}$  from *trans* to one of the *gauche* states and to the reverse rate  $\lambda_{gt}$  by

$$\lambda = 2p_t\lambda_{ig} + 2p_g\lambda_{gt} = 4p_t\lambda_{ig} \quad (13)$$

where the second equality follows from the principle of detailed balance. The isomerization rates  $\lambda_{ig}$  resulting from the least-squares fits of the plots for the four chains in Fig. 5(a) are listed in the fifth column of Table II. The isomerization rates decrease with chain extension.

In particular, it is noted from Fig. 5(a) that the most stretched chain (IV) exhibits distinctly lower slope  $\lambda$  indicative of a slower transition rate compared to the other three chains. At first glance, this feature appears contradictory to the trajectories displayed in Fig. 3. A closer examination reveals, however, that on a short-time scale this chain is, in fact, the one which exhibits the highest mobility as illustrated in Fig. 5(b). This figure which represents nothing else than the short-time portion of Fig. 5(a) clearly demonstrates the enhanced tendency of the

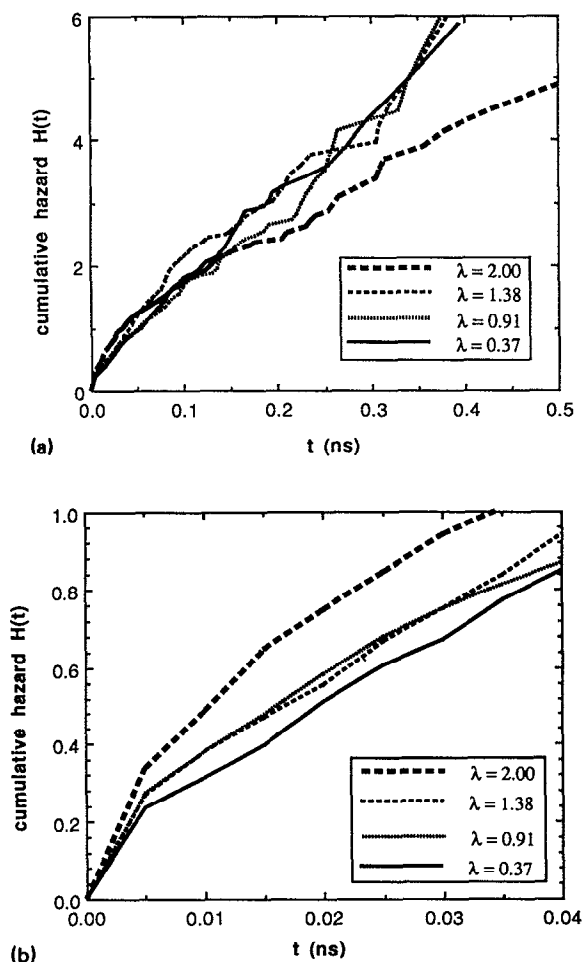


FIG. 5. (a) Time dependence of cumulative hazards  $H(t)$  for the simulated chains of various end-to-end separation. The lowest curve obtained for  $\lambda=2.00$  shows the low effective rate of isomerization of the most strained chain. (b) Short-time region of the hazard plot displayed in (a) indicating the enhanced tendency of the bonds in the most stretched chain to undergo back transitions to their original rotameric state.

chain IV to undergo high-frequency motions at short-time scales. The majority of those motions are, however, in the form of reverse transitions forcing the bond back to its original state and do not effectively contribute to the conformational relaxation of the chain. The effective rate of isomerization is portrayed by the long-time asymptotic slope of the cumulative hazards and is relatively low, as would be expected for a chain with considerably reduced degree of freedom.

### C. Equilibrium correlations between bond orientations

The equilibrium correlation between the orientations of bonds  $i$  and  $j$  along the chain is expressed by the order parameter or orientation function  $S$

$$S = \frac{1}{2} [3 \langle \mathbf{m}_i \cdot \mathbf{m}_j \rangle - 1] = \frac{1}{2} (3 \langle \cos^2 \alpha \rangle - 1), \quad (14)$$

where  $\mathbf{m}_i$  and  $\mathbf{m}_j$  are the unit vectors along the two bond vectors  $\mathbf{l}_i$  and  $\mathbf{l}_j$ , and  $\alpha$  is the angle between them. The angular brackets in Eq. (14) indicate both the time average

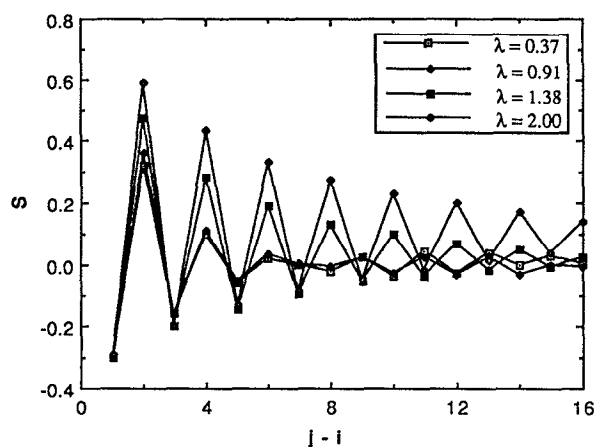


FIG. 6. Static orientational cross-correlation function  $S = \frac{1}{2} [3 \langle \mathbf{m}_i \cdot \mathbf{m}_j \rangle - 1]$  between bonds  $i$  and  $j$  as a function of the number  $j-i$  of intervening bonds, for the four chains with the indicated extensions, at 400 K. A strong even-odd effect enhanced by chain extension is observed.

for the pair of bonds  $i$  and  $j$  and the ensemble average over pairs of bonds with the fixed number  $j-i$  of intervening bonds. Figure 6 displays the decay of orientational cross correlations with an increasing number of intervening bonds for the four chains of different extensions. A sharp even-odd effect which persists over a large number  $j-i$  of intervening bonds is observed in the case of stretched chains. Strongest orientational correlations, positive or negative, occur in the case of the most strained chain (IV) as expected. It is interesting to note, on the other hand, that the orientational behavior of the contracted chain (I) closely resembles that of the unperturbed chain (II) and the orientational correlations between bonds vanish at about  $j-i=5$ , in those chains.

The influence of temperature on the degree of bond orientational correlations is illustrated in Fig. 7 where chain II is taken up. It is observed that the orientational correlations which vanish at about  $j-i=6$  at 400 K are

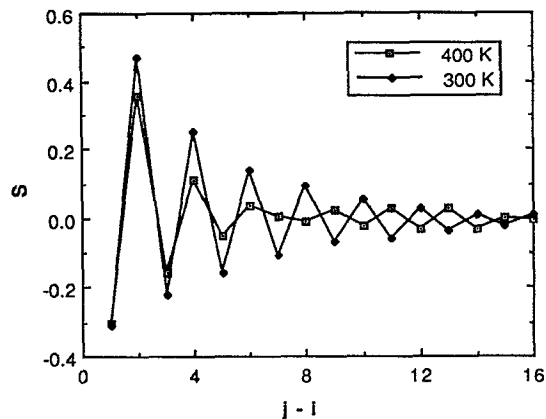


FIG. 7. Decrease in  $S$  with increasing temperature. Results are presented for the example chain II at the two simulation temperatures 300 and 400 K.

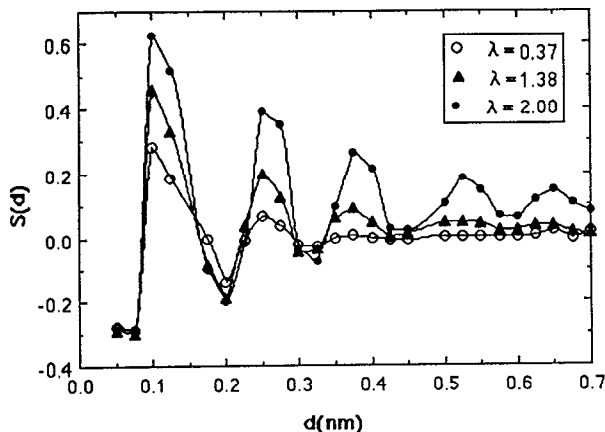


FIG. 8. Change in equilibrium orientational correlations  $S$  between pairs of bonds with increase in their separation  $d$ . The orientational correlation length does not extend beyond 0.5 nm except for the highly strained chain.

maintained until  $j-1 > 10$  with the decrease in temperature to 300 K.

An estimation of the orientational correlation distance between neighboring bonds may be performed by examining the change in the orientational cross-correlation function  $S$  with the distance separating the studied bonds. Figure 8 displays the variation of  $S$  with  $d$ , where  $d$  is taken as the distance between the midpoints of the bonds. Results reported in Fig. 8 are obtained by computing the average  $S$  values corresponding to intervals  $\Delta d$  of 0.025 nm. The curves exhibit oscillations which gradually level off with increasing  $d$  to the asymptotic values dictated by the particular chain extension. The lowest starting point reflects the almost tetrahedral bond angle between successive bonds and is not affected by chain extension. The effect of chain extension is distinguishable at longer separations. Strongest orientational correlations occur in the most stretched chain. The unperturbed chain exhibits the same behavior as the contracted chain I and is not explicitly displayed for clarity. The relative heights of the curves are in conformity with the ordering of their end-to-end separation. This dependence of  $S$  on  $d$  is characterized in all cases by a maximum correlation at a separation of about 0.12 nm, followed by a minimum at about 0.20 nm. Beyond 0.5 nm approximately, orientational correlations between bonds become negligibly small unless the chain is highly strained.

#### D. Time decay of bond-orientational autocorrelations

The first and second orientational autocorrelation functions (OACF) for a given bond  $i$  along the chain are given by the respective expressions

$$M_1(t) = \langle \mathbf{m}_i(0) \cdot \mathbf{m}_i(t) \rangle \quad (15)$$

and

$$M_2(t) = \frac{1}{2} \langle 3[\mathbf{m}_i(0) \cdot \mathbf{m}_i(t)]^2 - 1 \rangle. \quad (16)$$

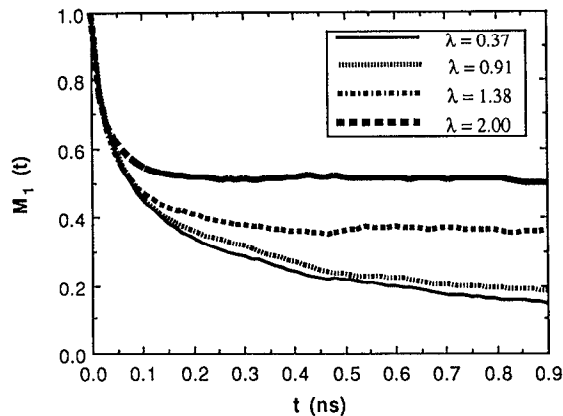


FIG. 9. Time decay of the first orientational autocorrelation function  $M_1(t)$  for internal bonds of simulated chains subject to indicated  $\lambda$  values. Deviations between curves arise mostly from differences between the equilibrium values asymptotically approached.

Here  $\mathbf{m}_i(0)$  and  $\mathbf{m}_i(t)$  represent the unit vectors associated with the initial and final states of the investigated bond vector.  $M_1(t)$  is related to dielectric relaxation process, whereas  $M_2(t)$  is observed in fluorescence anisotropy, NMR, and ESR experiments. In analogy to Eq. (14), the averages in Eqs. (15) and (16) are performed by taking both the ensemble and the time averages as

$$M_1(t) = \Delta t (n-2k)^{-1} (t_f - t)^{-1} \sum_{i=k}^{n-k} \sum_s \mathbf{m}_i(s\Delta t) \cdot \mathbf{m}_i(s\Delta t + t). \quad (17)$$

A similar expression applies to  $M_2(t)$ . The first summation includes all bonds devoid of end effects. The value  $k=10$  is safely used. The second summation is performed over discrete initial times  $s\Delta t$  with spacing  $\Delta t$ .  $s$  is varied from 0 to  $(t_f - t)/\Delta t$  for a total simulation duration of  $t_f$ , and  $\Delta t$  is chosen as 5000 fs. It is noted that the use of  $\mathbf{m}_i(s\Delta t)$  instead of  $\mathbf{m}_i(s\Delta t + t)$  in Eq. (17) yields at  $t=0$  the equilibrium property  $\langle \cos \alpha \rangle$ . Similarly,  $M_2(t)$  reduces to  $S$  upon substitution of  $t=0$  and  $j \neq i$ .

The time decay of the first OACF  $M_1(t)$  is displayed in Fig. 9. The initial decay rates are comparable in the chains with different extensions but the curves gradually separate as the equilibrium values are asymptotically approached. The distinction between the respective chains are even weaker if the second OACF  $M_2(t)$  is considered, as illustrated in Fig. 10. A measure of the dynamics of the chain excluding the effect of equilibrium constraints is the normalized OACF's:

$$M_i(t)_{\text{norm}} = [M_i(t) - M_i(\infty)] / [M_i(0) - M_i(\infty)], \quad i=1,2. \quad (18)$$

The time decay of the normalized first OACF is displayed in Fig. 11. It is clearly seen that bond reorientation is fastest in the most stretched chain indicating the occurrence of fast large amplitude motions on a localized scale. As far as the overall chain is concerned, on the other hand, the asymptotic high value of  $M_1(t)$  at long times in Fig. 9

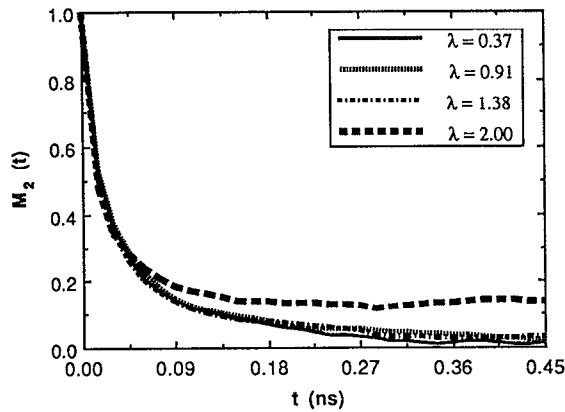


FIG. 10. Time decay of the second orientational autocorrelation function  $M_2(t)$  for internal bonds of simulated chains subject to indicated  $\lambda$  values.

shows that the ultimate orientational relaxation is considerably limited. This is a natural consequence of the imposition of an uniaxial tension holding the chain ends far above their unperturbed separation. Figure 11 shows that the bond reorientation is slowed down in the case of less extended chains.

Stretched exponential functions of the form<sup>23</sup>

$$M_i(t) = \exp\{-t/\tau_i\}^\beta \quad (19)$$

with  $0 < \beta < 1$  has been used in literature to approximate the time decay of correlation functions.  $\tau_i$  is the characteristic time for the specific relaxation process expressed by  $M_i(t)$ . Equation (19) may be rewritten as

$$\log[-\ln M_i(t)] = \beta \log t - \beta \log \tau_i \quad (20)$$

which permits an easier graphical analysis of the results. Plots of  $\log[-\ln M_i(t)]$  vs  $\log t$  are presented in Figs. 12 and 13 for  $i=1$  and 2, respectively. The analysis is mostly significant in the intermediate to long-time range inasmuch as a single exponential decay of correlation functions is

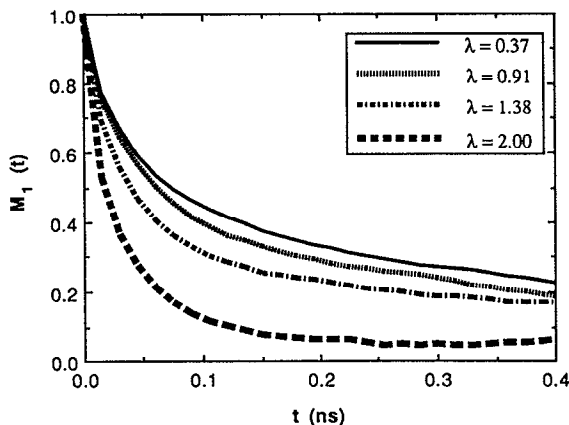


FIG. 11. Time dependence of normalized first OACF  $M_1(t)_{\text{norm}}$  which is a measure of local chain dynamics excluding equilibrium contributions. The loss of orientation of bonds occurs the fastest in the most strained chain and decreases gradually with decreasing end-to-end separation.

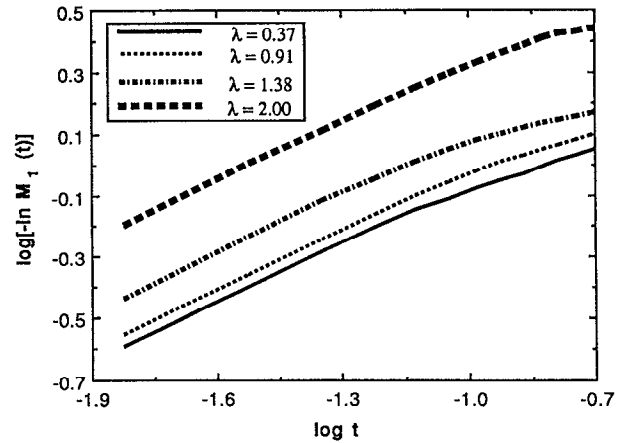


FIG. 12. Comparison of the time dependence of  $M_1(t)$  with the stretched exponential form according to Eq. (20). Best-fitting lines yield exponents  $\beta=0.46 \pm 0.03$  and the characteristic times listed in Table III.

operative in the two limits as  $t$  approaches zero or infinity. That the OACF's may be fairly well represented by stretched exponentials is seen from the approximately straight lines resulting from BD simulations. The exponents calculated from the slopes of the curves in Fig. 12 vary in the range  $0.46 \pm 0.03$ , smoothly increasing with chain extension. An exponent of  $\beta=0.55 \pm 0.04$  is obtained, on the other hand, from the best fitting lines in Fig. 13. The dependence on chain extension is mostly manifested by the vertical shifting of the curves which is directly related to the characteristic time  $\tau_i$ . It is noted that the characteristic times  $\tau_i$  associated with the first OACF exhibit a definite dependence on chain extension, whereas those corresponding to  $M_2(t)$  are relatively insensitive. Table III gives a summary of the exponents and characteristic times resulting from the BD trajectories of the four chains. A ratio of  $\tau_1/\tau_2$  of about 4 is obtained for the unperturbed chain. This ratio is found to decrease with increasing chain extension. Correlation times for the decay of  $M_1(t)$  and

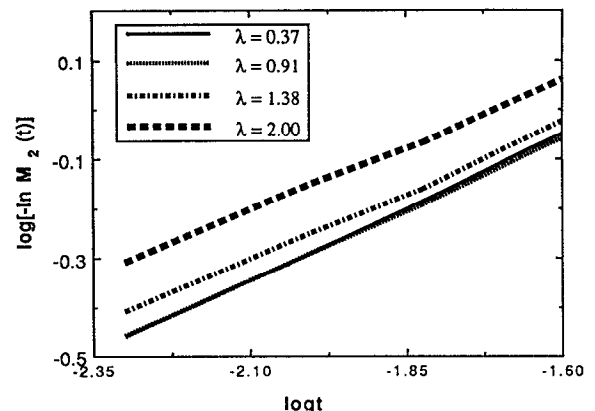


FIG. 13. Comparison of the time dependence of  $M_2(t)$  with the stretched exponential form. Exponents  $\beta=0.55 \pm 0.04$  are obtained from the best-fitting lines. The characteristic times and exponents for the four runs are listed in Table III.

TABLE III. Stretched exponential parameters for bond OACF's.

Run	$\lambda$	$M_1(t)$		$M_2(t)$	
		$\tau_2$ (ns)	$\beta$	$\tau_2$ (ns)	$\beta$
I	0.37	0.178	0.453	0.030	0.586
II	0.91	0.137	0.479	0.030	0.578
III	1.38	0.087	0.454	0.027	0.554
IV	2.00	0.026	0.477	0.020	0.523

$M_2(t)$  may alternatively be estimated from the times corresponding to  $1/e$  of their full relaxation. The correlation times obtained by this method exhibit the same dependence on chain extension. The ratio  $\tau_1/\tau_2$  is found to decrease linearly with chain extension, irrespective of the method of estimation of characteristic or correlation times, as illustrated in Fig. 14.

### E. Distribution of bond rotation and reorientation angles

Following the approach adopted by Takeuchi and Roe<sup>24,25</sup> for a detailed description of the time evolution of relaxational processes in polymers, time-dependent distribution functions is considered in the following. The evolution of bond torsional motions is described by the probability distribution function  $P(|\Delta\phi|, \Delta t)$  associated with the absolute changes in dihedral angles  $|\Delta\phi|$  occurring within the time interval  $\Delta t$ . Similarly,  $P(\Delta\alpha, \Delta t)$  represents the probability that a given bond undergoes a spatial reorientation of angle  $\Delta\alpha$  during a time span  $\Delta t$ .

Figures 15(a)–15(d) display the distribution functions  $P(|\Delta\phi|, \Delta t)$  of bond torsional motions obtained for the four chains of various extensions. The  $\lambda$  values corresponding to each of the labels (a)–(d) in Fig. 15 is indicated. The curves are drawn for  $\Delta t = 0.005, 0.060,$  and  $1.765$  ns in each case. The distribution functions are not normalized but rescaled such that  $P(|\Delta\phi| = 0^\circ, \Delta t) = 1$  for each of the chosen  $\Delta t$  values. Initially, the distribution function

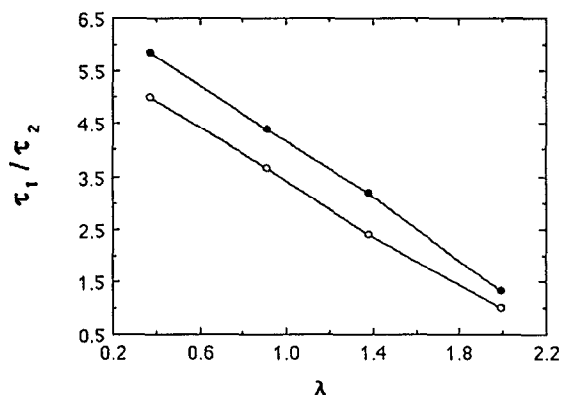


FIG. 14. Dependence of the ratio  $\tau_1/\tau_2$  on chain extension.  $\tau_1$  and  $\tau_2$  are obtained both from (i) the best fitting stretched exponentials (solid circles) and (ii) the  $1/e$  points of full decays of OACF's (open circles). Linear decrease of  $\tau_1/\tau_2$  with chain extension is observed irrespective of the method of approach.

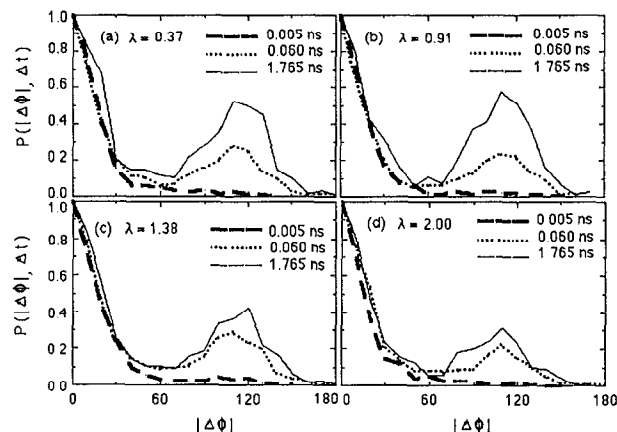


FIG. 15. Distribution function  $P(|\Delta\phi|, \Delta t)$  of absolute changes in dihedral angles within respective time intervals  $\Delta t$  of 0.005, 0.06, and 1.765 ns, for (a)  $\lambda = 0.37$ , (b)  $\lambda = 0.91$ , (c)  $\lambda = 1.38$ , and (d)  $\lambda = 2.00$ . The distribution functions are rescaled such that  $P(|\Delta\phi|, \Delta t) = 1$  at  $|\Delta\phi| = 0^\circ$ .

$P(|\Delta\phi|, \Delta t)$  is a dirac function with the pike at  $|\Delta\phi| = 0$ . With increase in the elapsed time the distribution is expected to broaden towards larger  $|\Delta\phi|$  values. However, the broadening does not occur in a Gaussian form but instead a second peak centered about  $|\Delta\phi| = 110^\circ$  appears which is indicative of the probable transition to another rotational isomeric state. In fact, the change in the torsional angle exactly reflects the rotational difference between the *trans* and *gauche* states of either sign in PE chains. At long times the equilibrium distribution of dihedral angles is gradually approached as revealed from the comparison of the uppermost curves in Figs. 15(a)–15(d) with those of Figs. 4(a)–4(d).

Figures 16(a)–16(d) display the evolution of bond reorientation in space. The distribution curves  $P(\Delta\alpha, \Delta t)$  are obtained from the angular displacement  $\Delta\alpha$  of bond vectors in space, by considering the same bond during two successive times with a delay of  $\Delta t$ . Curves are drawn for

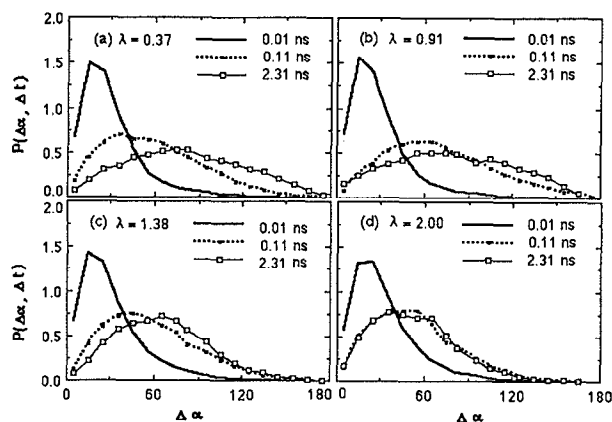


FIG. 16. Normalized probability distribution  $P(\Delta\alpha, \Delta t)$  for the reorientation of bond vectors by an angle  $\Delta\alpha$  within the time intervals of  $\Delta t = 0.01, 0.11,$  and  $2.31$  ns for (a)  $\lambda = 0.37$ , (b)  $\lambda = 0.91$ , (c)  $\lambda = 1.38$ , and (d)  $\lambda = 2.00$ .

$\Delta t=0.01, 0.11,$  and  $2.31$  ns. For an unbiased distribution of spatial reorientation the distribution curves should evolve from a dirac function at  $\Delta t=0$  to the functional form  $\frac{1}{2} \sin \Delta \alpha$  at long times. This is not the case as the chains are subject to fixed end-to-end separations that certainly constrain bond spatial reorientations. The unperturbed chain and the compressed chain obey comparable dynamics and approach the equilibrium distribution  $\frac{1}{2} \sin \Delta \alpha$  at long times, which is indicated by the dotted curve in parts Figs. 16(a) and 16(b). The bonds in the stretched chains, however, exhibit smaller  $\Delta \alpha$  values on the average, decreasing with chain extension. This clearly demonstrates the influence of the deformation of chain ends on the orientational mobility of the chain even at the scale of individual bonds.

#### IV. CONCLUDING REMARKS

In the present study, the BD simulation method has been employed for a systematic analysis of chain extension on the conformational and orientational dynamics of polymer chains. The picture of spatially frozen chain ends is conveyed by the classical model of network chains in which the junctions deform affinely with the macroscopic strain. A more realistic model would consider a distribution of end-to-end separations in the deformed state and the possible fluctuations of the constrained domains. Restriction of the analysis to fixed chain ends is a mathematical simplicity which is adopted for computational efficiency.

The hazard analysis of BD trajectories demonstrates that with increasing extension the effective isomerization rates decrease. The highly strained chain undergoes rapid rotational jumps although those are mostly in the form of back transitions forcing the bonds back to their original states and, hence, not contributing effectively to the conformational relaxation of the chain. Examination of the equilibrium correlations between bonds within the four chains of different extensions reveals the strong even-odd effect dominating the static cross correlations, in agreement with previous work.<sup>26</sup> The correlation length is about 0.5 nm in the unperturbed or weakly perturbed state but is larger in the highly stretched chain.

Dynamic orientational autocorrelations of bonds are described by the functions  $M_1(t)$  and  $M_2(t)$  differing in correlation times by a factor of about 4 in the case of unperturbed chains. This factor is found to decrease linearly with increasing end-to-end separation. Recent MD simulations of  $n$  alkanes in the bulk state by Takeuchi and Roe<sup>24</sup> yield a value of about 3 for the ratio  $\tau_1/\tau_2$  of the correlation times associated with  $M_1(t)$  and  $M_2(t)$  for bond reorientation. The small difference between the present results and those from MD simulations may be attributed to the influence of intermolecular constraints which are not presently considered. In fact, with increasing constraints at the chain ends, i.e., with increasing  $r$ , the ratio  $\tau_1/\tau_2$  is found to decrease linearly and approaches almost unity (indicative of large jump motions) in the highly strained chain. Previous analytical treatment based on the dynamic rotational isomeric states formalism leads<sup>27</sup>

to a ratio of about 1–1.5 which follows from the discrete  $120^\circ$  amplitude jumps inherently present in that approach.

The exponents  $\beta$  which satisfactorily reproduce the time decay  $M_1(t)$  and  $M_2(t)$  are found to assume the values  $0.46 \pm 0.03$  and  $0.55 \pm 0.04$ , respectively. For polyisoprene, recent BD simulations lead to  $\beta \approx 0.6$  for  $M_2(t)$  while  $\beta \approx 0.4$  for  $M_1(t)$  as measured in dielectric experiments and interpreted theoretically.<sup>28</sup> It is interesting to note that the exponents in the two different chains, polyethylene and polyisoprene, show comparable qualitative and quantitative dependence on the type of orientational autocorrelation function considered.

Time-dependent probability distribution functions describing the evolution of rotational and reorientational motions of the bonds indicate that the amplitudes of *rotational* motions are not affected by chain extension but their occurrence is reduced. Thus the location of the second peak in the distribution functions of Fig. 15 remains unchanged at about  $\Delta \phi = 112^\circ$  when increasing deformation but its height is reduced. The amplitudes of bond *reorientational* motions, on the other hand, are significantly diminished upon stretching of the chain as observed from the shift of the maxima in Fig. 16 to lower values with increasing chain extension. Thus, the long-time peak shifts from  $90^\circ$  for the unperturbed chain, to less than  $60^\circ$  for the highly strained chain.

#### APPENDIX

The position vector  $\mathbf{r}_i$  of the  $i$ th atom is a function of the generalized coordinates  $l_b, l_{i+1}, \theta_{i-1}, \theta_b, \theta_{i+1}, \phi_{i-1}, \phi_b, \phi_{i+1}$ , and  $\phi_{i+2}$ , as follows from the examination of Eqs. (1)–(3). Thus, the gradient of the overall potential  $V$  with respect to  $\mathbf{r}_i$  may be written as

$$\nabla_i V = \nabla_i \left( \sum_{k=i}^{i+1} V_b(l_k) + \sum_{k=i-1}^{i+1} V_\theta(\theta_k) + \sum_{k=i-1}^{i+2} V_\phi(\phi_k) \right). \quad (\text{A1})$$

It should be noted that in Eq. (A1), and in the following equations, the potential or the force having an undefined generalized coordinate as the argument [such as  $V_\theta(\theta_k)$  with  $k < 1$  or  $k \geq N$ ] is implicitly accepted to be equal to zero. Replacing in Eq. (A1) the negative gradients of the potential functions  $V_\xi$  (with  $\xi = b, \theta, \text{ or } \phi$ ) by the forces  $\mathbf{F}_\xi$  and inserting the results into the equation of motion (11), leads to

$$\beta d\mathbf{r}_i/dt = m^{-1} \left( \sum_{k=i}^{i+1} \mathbf{F}_b(l_k) + \sum_{k=i-1}^{i+1} \mathbf{F}_\theta(\theta_k) + \sum_{k=i-1}^{i+2} \mathbf{F}_\phi(\phi_k) \right) + \mathbf{A}_i(t). \quad (\text{A2})$$

The bond stretching forces  $\mathbf{F}_b(l_i)$  and  $\mathbf{F}_b(l_{i+1})$  which are associated with the deformation of the lengths of bonds  $i$  and  $i+1$  are given by

$$\mathbf{F}_b(l_i) = -k_b(1 - l_0/l_i)\mathbf{l}_i \quad (\text{A3})$$

for the displacement of atom atoms  $i$  in the range  $1 \leq i \leq N$ , and by

$$F_b(l_{i+1}) = k_b(1 - l_0/l_{i+1})l_{i+1} \quad (\text{A4})$$

for  $1 \leq i \leq N-1$ . On the other hand, the bond-bending forces on atom  $i$  arising from the distortions of the angles  $\theta_{i-1}$ ,  $\theta_i$ , and  $\theta_{i+1}$  are given, respectively, by

$$F_\theta(\theta_{i-1}) = -K_{\theta_{i-1}}(l_{i-1} - d_{i-1}^i l_i / l_i^2), \quad 2 \leq i \leq N \quad (\text{A5})$$

$$F_\theta(\theta_i) = -K_{\theta_i}[l_{i+1} - l_i + d_i^{i+1}(l_{i+1}/l_{i+1}^2 - l_i/l_i^2)], \quad 2 \leq i \leq N-1 \quad (\text{A6})$$

and

$$F_\theta(\theta_{i+1}) = K_{\theta_{i+1}}(l_{i+2} - d_{i+1}^{i+2} l_{i+1} / l_{i+1}^2), \quad 2 \leq i \leq N-2. \quad (\text{A7})$$

Here  $K_{\theta_m}$  and  $d_m^k$  are defined as

$$K_{\theta_m} \equiv k_\theta \frac{(\cos \theta_m - \cos \theta_0)}{l_m l_{m+1}} \quad (\text{A8})$$

and

$$d_m^k \equiv \mathbf{l}_m \cdot \mathbf{l}_k. \quad (\text{A9})$$

In order to write the rotational potential forces  $F_\phi(\phi_m)$ ,  $i-1 \leq m \leq i+2$ , in a more concise form, the following variables are introduced:

$$a_j^k = [l_j^2 l_k^2 - (d_j^k)^2], \quad (\text{A10})$$

$$A_1(i, j, k) = (d_{ij}^i - l_j^2 l_i) (d_i^k l_j^2 - d_j^k d_i^i) (a_j^i)^{-1} + (l_j^2 l_k - d_j^k l_j), \quad (\text{A11})$$

$$A_2(i, j, k) = (d_{ij}^i - l_j^2 l_i) (d_k^i l_i^2 - d_i^k d_k^i) (a_j^i)^{-1} + (l_i d_k^i - l_k d_j^i). \quad (\text{A12})$$

Using those variables, the bond rotational forces read as

$$F_\phi(\phi_{i-1}) = K_{\phi_{i-1}} A_1(i, i-1, i-2), \quad 3 \leq i \leq N \quad (\text{A13})$$

$$F_\phi(\phi_i) = K_{\phi_i} [A_2(i, i-1, i+1) - A_1(i+1, i, i-1) + A_2(i, i+1, i-1)], \quad 3 \leq i \leq N-1 \quad (\text{A14})$$

$$F_\phi(\phi_{i+1}) = -K_{\phi_{i+1}} [A_2(i+1, i, i+2) - A_1(i, i+1, i+2) + A_2(i+1, i+2, i)], \quad 3 \leq i \leq N-2 \quad (\text{A15})$$

and

$$F_\phi(\phi_{i+2}) = -K_{\phi_{i+2}} A_1(i+1, i+2, i+3), \quad 3 \leq i \leq N-3 \quad (\text{A16})$$

where the proportionality constant  $K_{\phi_m}$  is defined as

$$K_{\phi_m} \equiv -k_\phi (a_{m-1}^m a_m^{m+1})^{-1/2} \left( \sum_{i=1}^5 i a_i \cos^{i-1} \phi_m \right). \quad (\text{A17})$$

## ACKNOWLEDGMENT

Partial support by the Research Fund of Bogazici University, Grant No. 91P0029 is gratefully acknowledged.

<sup>1</sup> P. J. Flory, *Statistical Mechanics of Chain Molecules* (Interscience, New York, 1969).

<sup>2</sup> M. P. Allen and D. J. Tildesley, *Computer Simulation of Liquids* (Oxford University Press, London, 1989).

<sup>3</sup> M. Fixman, *J. Chem. Phys.* **69**, 1527 (1978).

<sup>4</sup> M. Fixman, *J. Chem. Phys.* **69**, 1538 (1978).

<sup>5</sup> J. H. Weiner and M. R. Pear, *Macromolecules* **10**, 317 (1977).

<sup>6</sup> E. Helfand, *J. Chem. Phys.* **69**, 1010 (1978).

<sup>7</sup> M. R. Pear and J. Weiner, *J. Chem. Phys.* **71**, 212 (1979).

<sup>8</sup> M. R. Pear and J. H. Weiner, *J. Chem. Phys.* **72**, 3939 (1980).

<sup>9</sup> R. M. Levy, M. Karplus, and J. A. McCammon, *Chem. Phys. Lett.* **65**, 338 (1979).

<sup>10</sup> E. Helfand, Z. R. Wasserman, and T. A. Weber, *J. Chem. Phys.* **70**, 2016 (1979).

<sup>11</sup> E. Helfand, Z. R. Wasserman, and T. A. Weber, *Macromolecules* **13**, 526 (1980).

<sup>12</sup> M. Bishop and J. H. R. Clarke, *J. Chem. Phys.* **91**, 6345 (1989).

<sup>13</sup> M. Bishop and J. H. R. Clarke, *J. Chem. Phys.* **93**, 1455 (1990).

<sup>14</sup> M. Bishop and J. P. C. Michels, *J. Chem. Phys.* **84**, 447 (1986).

<sup>15</sup> E. Helfand, Z. E. Wasserman, T. A. Weber, J. Skolnick, and J. H. Runnels, *J. Chem. Phys.* **75**, 4441 (1981).

<sup>16</sup> M. Fixman, *J. Chem. Phys.* **78**, 1954 (1983).

<sup>17</sup> J. L. Garcia Fernandez, A. Rey, J. J. Freire, and I. Fernandez de Piérola, *Macromolecules* **23**, 2057 (1990).

<sup>18</sup> A. Rey, J. J. Freire, and J. Garcia de la Torre, *J. Chem. Phys.* **90**, 2035 (1989).

<sup>19</sup> D. L. Ermak and J. A. McCammon, *J. Chem. Phys.* **69**, 1352 (1978).

<sup>20</sup> D. B. Adolf and M. D. Ediger, *Macromolecules* **24**, 5834 (1991).

<sup>21</sup> E. Helfand, *Bell Syst. Tech. J.* **58**, 2289 (1979).

<sup>22</sup> J. P. Ryckaert and A. Bellemans, *Chem. Phys. Lett.* **30**, 123 (1975).

<sup>23</sup> G. Williams, *Adv. Polym. Sci.* **33**, 59 (1979).

<sup>24</sup> H. Takeuchi and R.-J. Roe, *J. Chem. Phys.* **94**, 7446 (1991).

<sup>25</sup> H. Takeuchi and R.-J. Roe, *J. Chem. Phys.* **94**, 7458 (1991).

<sup>26</sup> I. Bahar and B. Erman, *J. Chem. Phys.* **88**, 1228 (1988).

<sup>27</sup> I. Bahar, B. Erman, and L. Monnerie, *Macromolecules* **22**, 431 (1989).

<sup>28</sup> I. Bahar, B. Erman, F. Kremer, and E. W. Fischer, *Macromolecules* **25**, 816 (1992).